



Research
Laser Micro/Nano-Manufacturing—Article

Sub-Diffraction Limit Quantum Metrology for Nanofabrication

Wenyi Ye ^{a,b,c,d,#}, Yang Li ^{a,b,c,#}, Lianwei Chen ^{a,b,#}, Mingbo Pu ^{a,b,c,d}, Zheting Meng ^{a,b,c,d}, Yuanjian Huang ^e, Hengshuo Guo ^f, Xiaoyin Li ^{a,b,c}, Yinghui Guo ^{a,b,c,d}, Xiong Li ^{a,b,c,d}, Yun Long ^{a,b,c,d}, Emmanuel Stratakis ^{g,h}, Xiangang Luo ^{a,b,d,*}



^a National Key Laboratory of Optical Field Manipulation Science and Technology, Chinese Academy of Sciences, Chengdu 610209, China

^b State Key Laboratory of Optical Technologies on Nano-Fabrication and Micro-Engineering, Institute of Optics and Electronics, Chinese Academy of Sciences, Chengdu 610209, China

^c Research Center on Vector Optical Fields, Institute of Optics and Electronics, Chinese Academy of Sciences, Chengdu 610209, China

^d College of Materials Science and Opto-Electronic Technology, University of Chinese Academy of Sciences, Beijing 100049, China

^e Department of Communication Science and Engineering, Fudan University, Shanghai 200438, China

^f Tianfu Xinglong Lake Laboratory, Chengdu 610299, China

^g Institute of Electronic Structure and Laser, Foundation for Research and Technology-Hellas, Heraklion 71110, Greece

^h Department of Physics, University of Crete, Heraklion 70013, Greece

ARTICLE INFO

Article history:

Received 8 September 2024

Revised 22 February 2025

Accepted 3 April 2025

Available online 22 April 2025

Keywords:

Nanofabrication

Precision measurement

Diffraction limit

Quantum metrology

ABSTRACT

Optical monitoring of object position and alignment with nanoscale precision is critical for ultra-precision measurement applications, such as micro/nano-fabrication, weak force sensing, and microscopic imaging. Traditional optical nanometry methods often rely on precision nanostructure fabrication, multi-beam interferometry, or complex post-processing algorithms, which can limit their practical use. In this study, we introduced a simplified and robust quantum measurement technique with an achievable resolution of 2.2 pm and an experimental demonstration of 1 nm resolution, distinguishing it from conventional interferometry, which depended on multiple reference beams. We designed a metasurface substrate with a mode-conversion function, in which an incident Gaussian beam is converted into higher-order transverse electromagnetic mode (TEM) modes. A theoretical analysis, including calculations of the Fisher information, demonstrated that the accuracy was maintained for nanoscale displacements. In conclusion, the study findings provide a new approach for precise alignment and metrology of nanofabrication and other advanced applications.

© 2025 THE AUTHORS. Published by Elsevier LTD on behalf of Chinese Academy of Engineering and Higher Education Press Limited Company. This is an open access article under the CC BY-NC-ND license (<http://creativecommons.org/licenses/by-nc-nd/4.0/>).

1. Introduction

Optical methods for precisely measuring small displacements are critical for various applications, including nanofabrication, nanomonitoring, weak force sensing, microscopy, and micro/nano-fabrication [1]. High-quality displacement sensors, such as membrane-in-the-middle optomechanical cavities and macroscopic interferometers, have enabled significant achievements, including the observation of motional quantum ground states, gravitational waves, and single phonons [2–7]. Early displacement measurements relied on mechanical tools, such as calipers and micrometers, which lacked the precision required for micron- or nanometer-scale measurements. Optical displacement measure-

ment technology has since become the cornerstone of precision measurements [8,9]. Advanced techniques, such as back-action-evading measurements [10], variational read-out [11], polarization-encoded metasurfaces [12,13], linear photonic gears [14], and squeezed light injection [15,16], have been developed. Interferometers and grating displacement measurement systems [17] are widely used, with the latter utilizing the diffraction principle of gratings to measure displacement. However, long-range measurements necessitate the fabrication of nanostructures on large scales up to meters, which can be costly. Interferometers offer high resolution down to the nanometer level, but they can be affected by accumulated errors owing to noise from media turbulence during long-range and long-duration measurements.

Achieving nanoscale resolution for long-range measurements is challenging, particularly when simple optical architectures, robustness, cost-effectiveness, and ease of integration are required for the nanofabrication processes. The diffraction limit, described

* Corresponding author.

E-mail address: lxg@ioe.ac.cn (X. Luo).

These authors contributed equally to this work.

by the Rayleigh's criterion [18], poses a fundamental challenge for many optical systems. The particle nature of the photons introduces randomness into the detection of precise locations. To account for noise in the resolution, the theory of statistical inference provides a useful framework. Tsang et al. [19,20] proposed a groundbreaking technique based on the quantum theory of super resolution, which could estimate the separation of two incoherent optical point sources by defying Rayleigh's criterion. This method has been widely explored for super-resolution microscopy and telescope imaging [21–43].

In this study, we extended the two-source quantum imaging theory to accurately measure the displacements of a single optical beam. In the context of quantum optics, quantum metrology, and statistical analysis, we experimentally demonstrated measurements with a precision of approximately 1/290 000 of the diffraction limit (calculated as the measurement accuracy divided by the size of the zero-order airy disk at the focus). Our experimental setup involved designing a mode-conversion pattern and fabricating a corresponding metasurface [40,42,44] substrate; this metasurface, mounted on a one-dimensional displacement nanostage, allowed transverse displacements. A Gaussian beam incident on the metasurface was converted into higher-order transverse electromagnetic mode (TEM) modes, which were detected using optical sensors. By analyzing the displacement within an extended quantum framework and calculating the Fisher information for nanoscale displacements, we found that the ability to detect the position of the metasurface remained accurate even below the diffraction limit. In practice, by detecting the intensity of the separated TEM modes, we could measure the displacement of the metasurface with a precision of 1 nm, which was not the theory limit but constrained only by the limitations of the nanostage. This approach is versatile because a mode-conversion pattern can be fabricated on any type of surface. Further, we proposed two additional setups: an integrated on-chip displacement sensor for 1 nm resolution measurements across various substrates and a multi-dimensional feedback system with sub-nanometer alignment accuracy for processes at 7 nm and below in advanced integrated circuit manufacturing.

2. Methods

2.1. Fabrication

Several approaches exist for fabricating metasurfaces [45–55]. The fabrication method employed in this study was a recently proposed technique that emphasized high robustness by creating meta-atoms within a transparent substrate. A detailed description of the fabrication process, along with its advantages and limitations, can be found in Ref. [56]. The metasurface utilized laser-induced birefringence nanopores within silica glass, with an average nanopore diameter ranging from 35 to 45 nm. This metasurface operated based on geometric phase modulation, enabling us to tune the phase shift from 0 to 2π by adjusting the incident light polarization. Sections S1 and S2 in Appendix A present the results of the laser source stability tests and the raw data from the experimental measurements, respectively. An optical image of the metasurface and an SEM image of the nanopores is provided in Section S3 in Appendix A. Sections S4 and S5 in Appendix A present a list of the experimental equipment, and a comparison of the parameters between previous excellent measurement methods and our proposed approach, respectively.

2.2. Principle of measurement and theoretical simulation

Figs. 1(a) and (b) present schematics of the proposed metasurface-based optical mode conversion configuration. In this

setup, the mode conversion is facilitated by a specially designed metasurface that imparts a π phase shift to half of the incident beam. On the spatial plane of the metasurface, the amplitude distribution of the light wave can be represented as a Hermite–Gaussian mode, corresponding to the TEM00 mode as the initial signal. The complex amplitude (u_{mn}) of the incident light is given by Eq. (1) [57]:

$$u_{mn} \approx C_{mn} H_m(x) H_n(y) e^{-\frac{(x^2+y^2)}{2}} \quad (1)$$

where m and n denote the number of modes in the x and y directions, respectively, and C_{mn} is the constant associated with m and n , which is 1. x and y denote the spatial coordinates corresponding to physical positions in real space. $H_m(x)$ and $H_n(y)$ are Ermitian polynomials, which can be expressed as

$$H_m(x) = (-1)^m e^{x^2} \frac{d^m (e^{-x^2})}{dx^m} \quad (2)$$

$$H_n(y) = (-1)^n e^{y^2} \frac{d^n (e^{-y^2})}{dy^n} \quad (3)$$

Therefore, the fundamental mode TEM00 complex amplitude u_{00} can be simplified as follows:

$$u_{00} \approx e^{-\frac{(x^2+y^2)}{2}} \quad (4)$$

As previously mentioned, a π phase shift is essential for the desired mode conversion. This can be achieved by fabricating a metasurface using liquid crystal polymer films [58,59] with different fast axis orientations and dividing the entire metasurface into two regions where the fast axes are perpendicular to each other. By adjusting the relative positions of the metasurface and incoming light beams, the proportion of power entering the 0- and π -phase regions can be precisely controlled. The metasurface was mounted on a displacement stage with a resolution of 1 nm to allow for fine adjustments. According to the Fresnel diffraction principle, the transmitted complex amplitude $t(x_0, y_0)$ of the diffraction screen Σ can be expressed as

$$t(x_0, y_0) = A(x_0, y_0) e^{j\varphi(x_0, y_0)} \quad (5)$$

where (x_0, y_0) denotes the spatial coordinates on the diffraction screen, $A(x_0, y_0)$ denotes the amplitude equal to 1, and $\varphi(x_0, y_0)$ denotes the phase (half of which is 0, and half of which is π), which is separated by 0 to π phase-shifted line (PSL). j denotes the imaginary unit. We define $u(x_0, y_0)$ as the complex amplitude of the light field on the diffractive surface ε , and $u(x_0, y_0)$ as the complex amplitude of the r-points on the observation surface.

$$u(x_0, y_0) = u_{00} \times t(x_0, y_0) \quad (6)$$

Fig. 1(b) illustrates the diffraction process of the incident beam through the metasurface, resulting in the optical field p observed on the detection screen, as described by the Fresnel diffraction integral in Eq. (7):

$$u(x, y) = \frac{e^{jkd}}{j\lambda d} \int \int_{-\infty}^{\infty} u(x_0, y_0) e^{\left\{ \frac{jk}{2d} [(x-x_0)^2 + (y-y_0)^2] \right\}} dx_0 dy_0 \quad (7)$$

where λ is the wavelength of the incident light, $k = 2\pi/\lambda$ is the wave number, and d is the distance from the diffracting surface to the viewing surface. Eq. (7) can be rewritten as

$$u(x, y) = \frac{e^{jkd}}{j\lambda d} e^{\left[\frac{jk}{2d} (x^2 + y^2) \right]} \int \int u(x_0, y_0) e^{\left\{ \frac{jk}{2d} (x_0^2 + y_0^2) \right\}} \times e^{\left[-j2\pi \left(\frac{x_0 x}{d} + \frac{y_0 y}{d} \right) \right]} dx_0 dy_0 \quad (8)$$

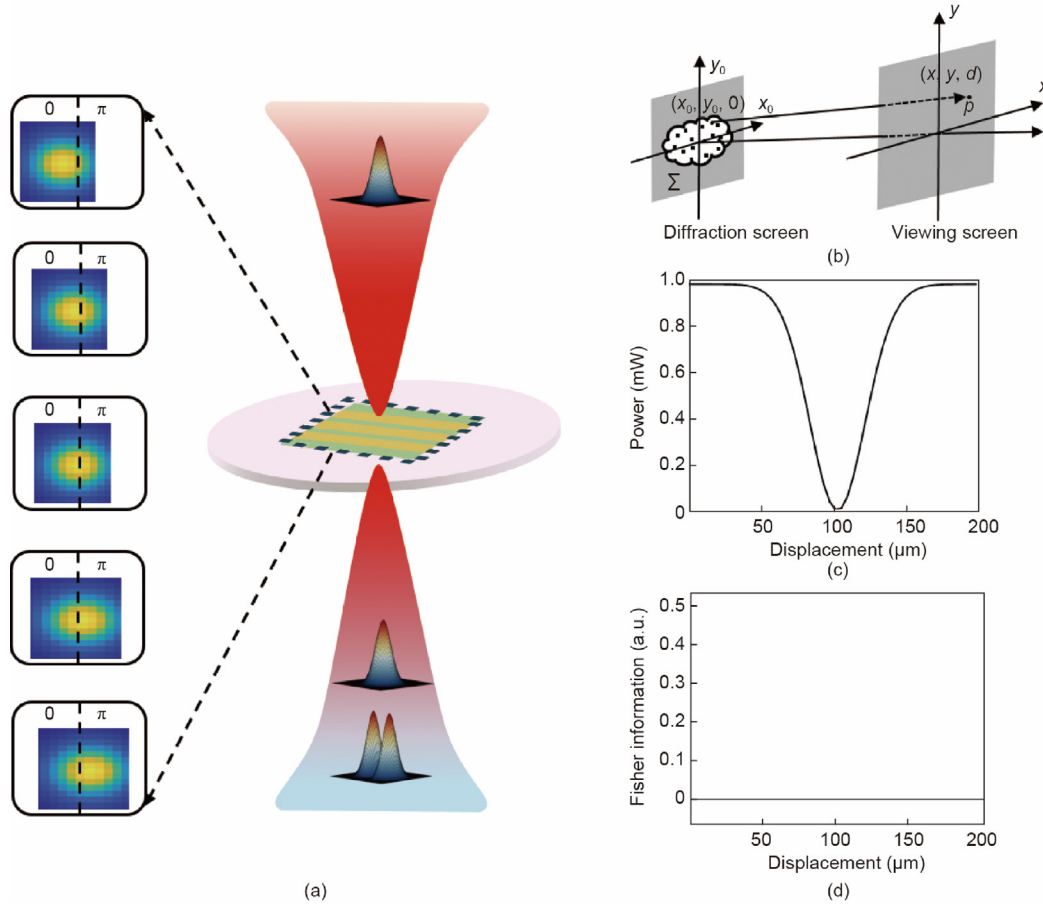


Fig. 1. Metasurface-based quantum displacement measurement. (a) Working principle of metasurface displacement measurement can be understood as the detection of the power of different modes of the converted light. The incident irradiated on the metasurface and converted into different modes. When the metasurface is shifted, the power of these converted modes changes. The displacement can be characterized by detecting and comparing the power of the corresponding modes. (b) Schematic of diffraction and coordinates after incident light passing through the metasurface. Σ is the diffraction screen, and p is the detected spot on the observation plane. (c) Simulation of primary mode output power vs the displacement. (d) Calculated quantum Fisher information of the system.

From Eq. (8), the complex amplitude of the light field on the observation screen is considered as the Fourier transform of the complex amplitude of the light field after passing through the diffraction screen. Fig. 1(c) shows the simulation results based on this theory. The intensity distribution of the laser mode conversion was modeled using a simplified mathematical approach, where the mode conversion efficiency was assumed to follow a Gaussian distribution, representing a scenario in which a single-mode fiber was used as the receiver. In this model, the coupling efficiency η is determined by the overlap integral between u_{00} and the fiber's transmission mode, which closely approximates a Gaussian profile. As shown in Eq. (9):

$$\eta = \frac{|\iint u_{00} \times u(x, y) dx dy|^2}{\iint |u_{00}|^2 dx dy \times \iint |u(x, y)|^2 dx dy} \quad (9)$$

According to optical theory, an ideal parallel light beam or spherical wave should be focused on a diffraction-limited point after passing through an ideal optical lens. However, because of various aberrations, the actual size of the focus depends on several parameters, including the wavelength, focal length, and diameter of the optical beam. This focus size limitation poses a bottleneck in the resolution of optical detection. In the early 1960s, Helstrom summarized and generalized the theory of quantum detection. In recent years, many scientists have applied quantum theory to address imaging challenges, with Fisher information [60,61] as a key tool in these studies. In this section, we analyze the measure-

ment accuracy limit using quantum Fisher information. As shown in Fig. 1(c), the light intensity on the receiving screen is continuously distributed, allowing us to calculate the Fisher information for the system using Eq. (10), where θ represents the displacement of the metasurface:

$$F_\theta = \int_{-\infty}^{+\infty} dx \frac{1}{u} \left(\frac{\partial u}{\partial \theta} \right)^2 \quad (10)$$

where u represents the optical intensity collected by the fiber, which varies as a function of the displacement of the metasurface. According to Eq. (9), only the TEM00 mode light can be coupled to the single mode fiber. Therefore, we denote the probability of receiving the TEM00 mode as q , the probability of non-TEM00 modes as $(1 - q)$, and the corresponding Fisher information as

$$F_\theta = \frac{1}{q} \left(\frac{\partial q}{\partial \theta} \right)^2 + \frac{1}{1 - q} \left[\frac{\partial(1 - q)}{\partial \theta} \right]^2 \quad (11)$$

Fig. 1(d) illustrates the Fisher information profile of our system. The results show that even if the displacement of the metasurface is below the diffraction limit, the quantum Fisher information of the system does not change with displacement, which indicates that the accuracy of the measurement is consistent in the sub-diffraction region.

2.3. Experimental setup and process of displacement measurement

As shown in Fig. 2(a), an experimental system was constructed to demonstrate high-precision displacement measurements in the

horizontal direction. The collimated linearly polarized light output from the fiber laser was split into two beams of equal power using a beam splitter with two diaphragms to ensure that the beams were aligned at the same height. To measure laser power, one beam was passed through a linear polarizer and directly detected using a power meter. The metasurface, designed based on the Pancharatnam–Berry (PB) phase, required the incident light to be left circularly polarized. Therefore, the other beam was directed through a linear polarizer and a $\lambda/4$ wave plate after the beam splitter. To record the initial power incident on the metasurface, the beam was further split using another beam splitter and detected using a power meter. To enhance measurement accuracy, the left circularly polarized beam was focused onto the metasurface using a lens with a focal length of 250 mm. The metasurface was mounted on a high-precision motorized displacement stage (Sigma SHRC-203, SIGMAKOKI, Japan) capable of generating transverse displacements with a 1 nm resolution, controlled by a computer. The light converted by the metasurface was collimated through another 250 mm lens and coupled into a single-mode fiber using a collimator. The optical fiber was connected to a power meter to measure the laser power of the base mode at different metasurface displacements. Fig. 2(b) presents several sets of experimental data that reproduce the distribution pattern of the fitted curve shown in Fig. 1(c), as described by Eq. (10).

During the measurements, we first identified the boundary between the 0- and π -phase regions by scanning horizontally from the edge of the metasurface. The boundary was located by detecting the minimum point of the light power. Subsequently, we collected several sets of data and observed that the slope of the curve reached its maximum when the power decreased to approximately half of the incident power. This point corresponded to the highest resolution of the displacement measurement.

3. Long ranges and 1 nm resolution displacement measurement results

We quantified the measurement results for different small displacements to characterize the resolution of the system. As shown in Fig. 3(a), the metasurface performance was measured at various step sizes. The horizontal black lines in Fig. 3(a) indicate the movements of the metasurface at the piezoelectric level with step sizes

of 5 and 2 nm. The experimental data clearly demonstrate that the 2 nm steps are easily distinguishable. To further highlight the measurement capabilities of the proposed system, we conducted multiple repetitions of 1 nm displacements in the most sensitive region of the setup and analyzed the power difference before and after each displacement. This approach allowed us to precisely measure smaller displacement steps. Fig. 3(b) presents histograms of the power distribution at four different locations. For each histogram, 450 measurement points were collected to compute the average, and the histograms were fitted using a Gaussian function. Each horizontal black line represents the average detected optical power following a 1 nm horizontal shift.

The experimental data demonstrated that the 1 nm displacement was clearly and consistently resolved. The overall system error measurements are provided in the Appendix A. Notably, the 1 nm is not the limiting accuracy of the system; an even higher measurement precision can be achieved with a more stable experimental setup, higher-precision detector, and lock-in amplifier to minimize ambient noise.

We further investigated the factors affecting the accuracy of the displacement measurements and demonstrated their capability for high-precision, large-range displacements across a wide area of the metasurface. Because the detection accuracy depended on the maximum slope of the power curve, achieving cross-scale high-precision displacement measurements over an extended range was possible. We analyzed the effects of the spot size and rotation angle on the displacement accuracy. Fig. 4(a) shows the overall power conversion results of the system for different displacement segments, sampled across full ranges of 235 and 2030 μm , respectively. We observed that when half of the incident beam fell within the 0-phase region of the metasurface and the other half within the π -phase region, the energy did not attenuate to zero as predicted by the theoretical simulation in Fig. 1(c). This deviation was attributed to fabrication imperfections in the metasurface, which resulted in a conversion efficiency of less than 100%. Importantly, the size of the metasurface is a critical limiting factor for these measurements; the metasurface must completely cover the focal spot. Fig. 4(b) presents the measurement results for 1 and 10 nm displacements obtained in the most sensitive regions of the system at the 235 and 2030 μm ranges. The data indicate that the measurement accuracy increases as the spot size decreases, and

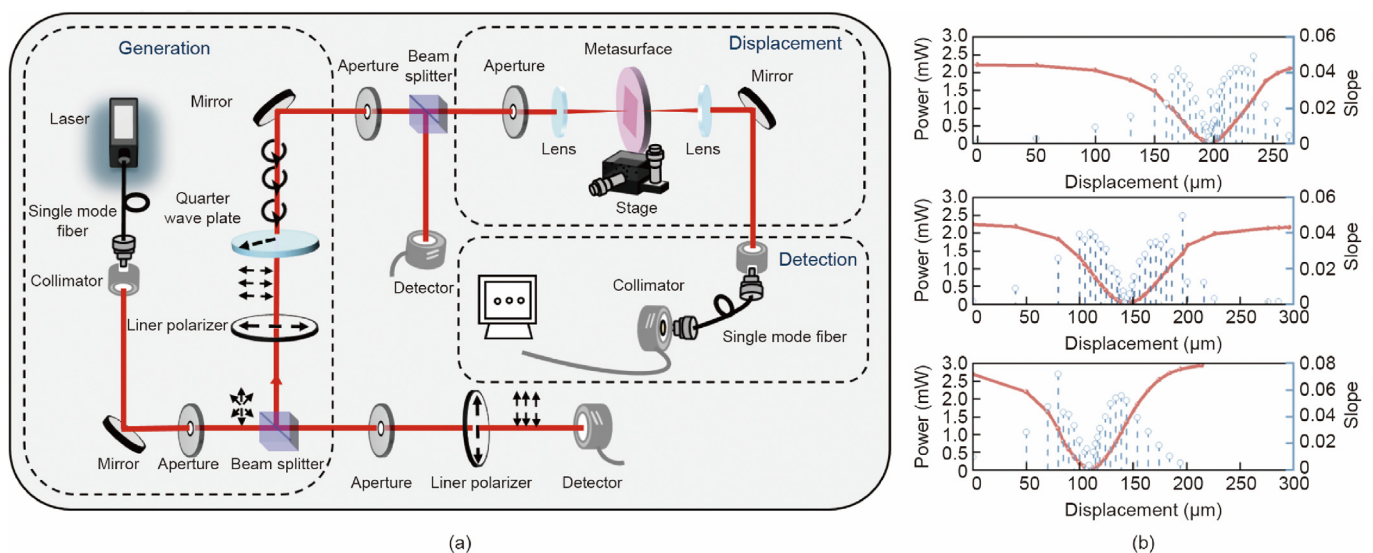


Fig. 2. Experimental implementation of metasurface quantum displacement setup. (a) Schematic and components of experimental layout. (b) Experimental results corresponding to the output power of different spot sizes for displacement measurement; the maximum value of the slope of the curve occurs at the position corresponding to half of the incident light power.

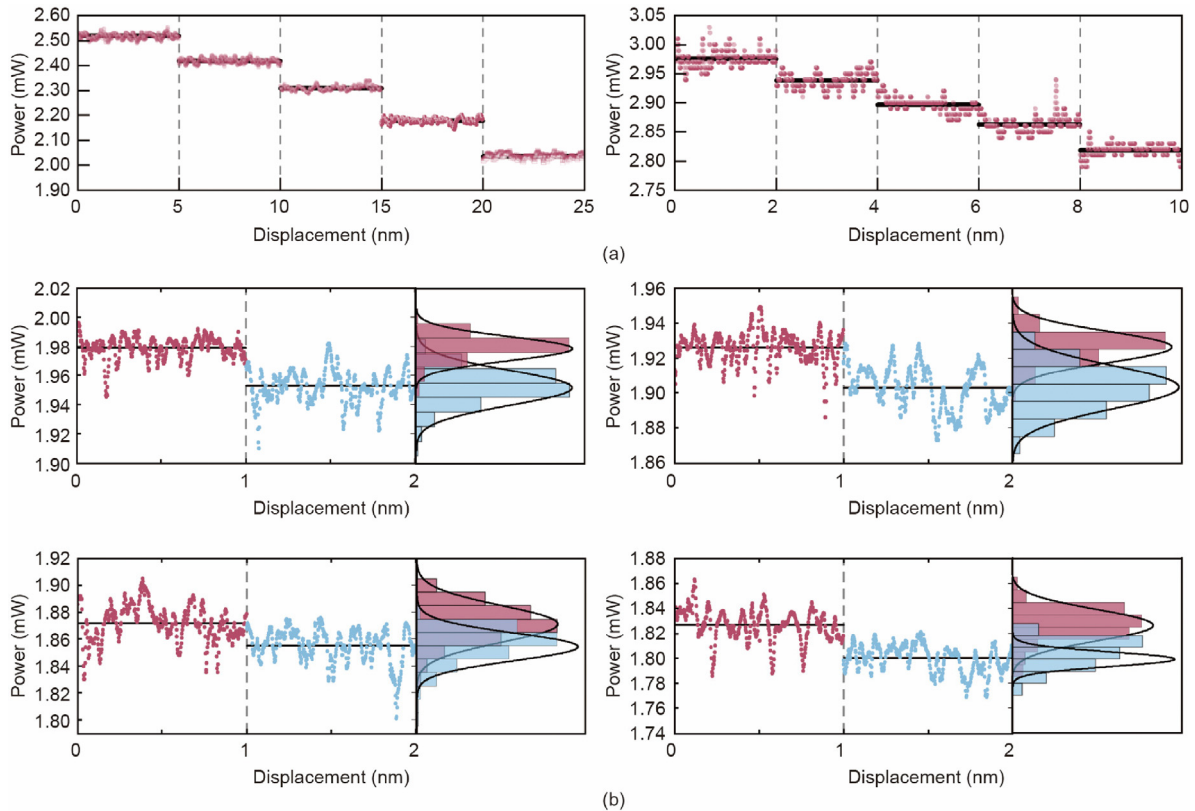


Fig. 3. (a) Results of metasurface at different displacement steps of 5 nm (left) and 2 nm (right). (b) Results at 1 nm displacement. The motion can be well resolved.

smaller spot sizes result in more concentrated power and higher conversion efficiency for the same step scan.

In addition, we analyzed the effect of the angle on the measurement system. To ensure optimal spot incidence on the metasurface and improve optical mode conversion efficiency, the metasurface was mounted on a rotating stage. Figs. 4(c) and (d) show the results at 79° (relative to the center of rotation) and $78^\circ40'$, respectively. At 79° , where the spot is optimally incident, the metasurface sweeps perpendicularly across the center of the spot, converting most of the TEM₀₀ mode to the TEM₁₀ mode, with the power reaching a minimum. As a comparison, after rotating the stage by 20 arcmin (approximately 1/4 of the minimum precision of the mechanical rotary stage) and returning the piezoelectric displacement stage to its initial position, the incident power increased by a factor of 110 compared to the 79° position. This significant increase indicated poor conversion because the power that should have bottomed out remained high.

4. Discussion

Here, we discuss possible layouts for various applications, as illustrated in Fig. 5. Ultra-precision measurement technology remains essential for numerous scientific endeavors, including laser micro/nano-processing, lithography positioning, and interstellar exploration. The pursuit of increasingly accurate measurements of physical quantities has become a central objective in modern science and technology. For instance, in chip fabrication, extreme ultraviolet (EUV) lithography is a fundamental technology that advances semiconductor manufacturing toward smaller nodes, such as 5 and 3 nm. Precision displacement measurements play a critical role in ensuring accurate alignment, optical stability, and wafer stage positioning. High-precision interferometric tech-

niques are widely employed to monitor and correct motion in real time, effectively minimizing overlay errors and enhancing wafer stage positioning accuracy. In comparison with conventional laser interferometry, our method offers easier integration and a simpler operating principle while achieving picometer-level resolution. The proposed metasurface-mode decomposition displacement measurement system is employed for real-time monitoring of the wafer stage position. Our future work will focus on extending this approach to large-range measurements with six degrees of freedom. Moreover, this effectively eliminates the accumulation of errors inherent in interferometric measurements and offers a more cost-efficient solution, as illustrated in Fig. 5(b).

Precision measurements also play a critical role in laser beam metrology. Fluctuations in laser beam pointing can have detrimental effects in many high-precision optical applications such as super-resolution imaging microscopy, nanolithography, and optical tweezers. Over long propagation paths, the pointing of the laser beam fluctuates owing to nonlinear effects such as thermal expansion, mechanical vibration, and spatiotemporal inhomogeneities. These fluctuations are classified as positional (x, y) or angular (θ, φ) beam deviations. Researchers commonly use position-sensitive and four-quadrant detectors to monitor changes in the positions and orientations of laser beams. As shown in Fig. 5(b), the proposed scheme is simple, robust, and easy to integrate, making it highly suitable for these applications. These sensors can accurately detect small changes in the beam position, enabling real-time feedback control to maintain beam stability.

In this study, we used a detector with a minimum measurement power of 20 pW and a slope of $K_{\max} = 91.8 \text{ W}\cdot\text{m}^{-1}$ at the most sensitive point of the system when focusing with a 25 cm lens; according to Eq. (12), we calculated the detection sensitivity of the achievable resolution to be 2.18 pm. Our measurement scheme

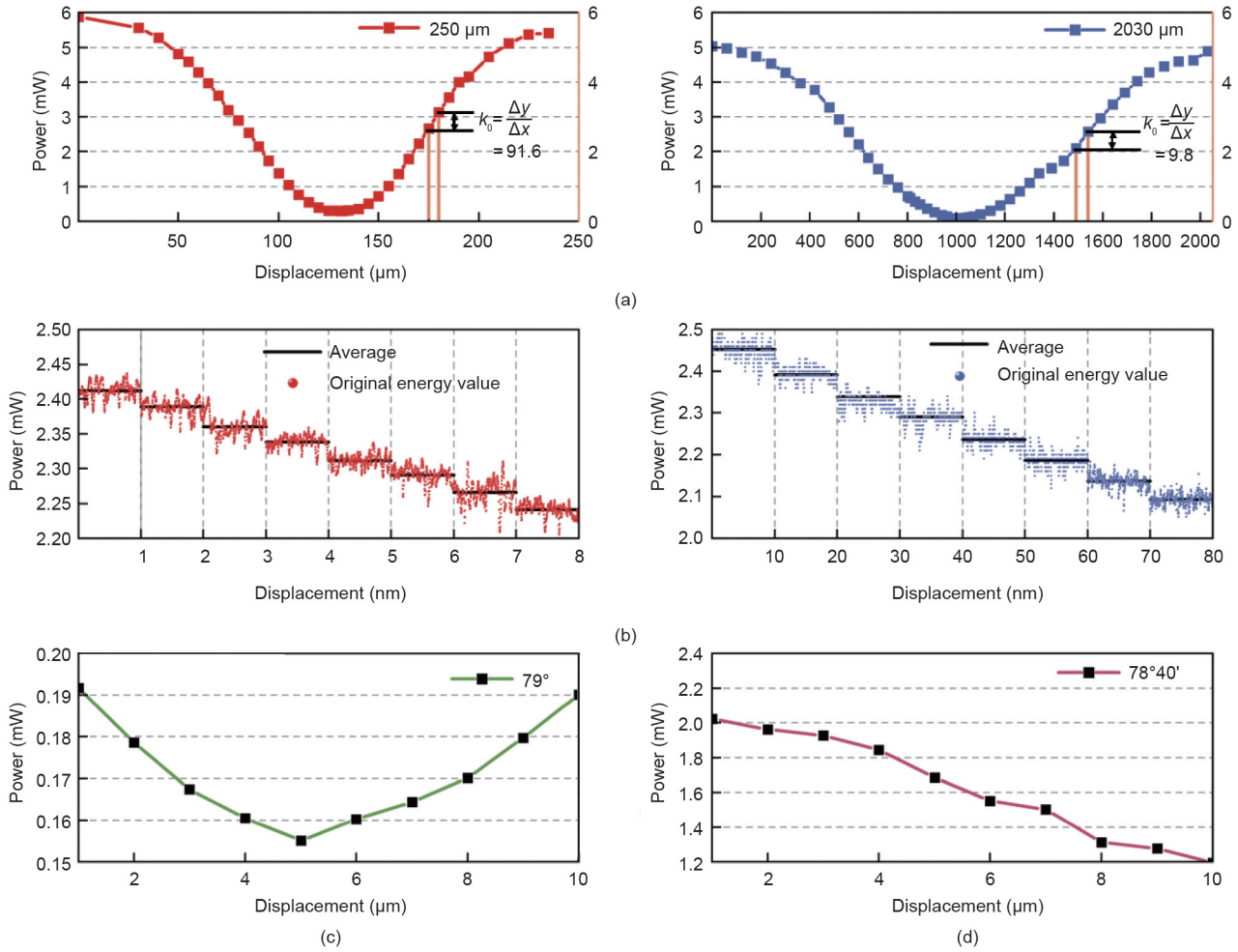


Fig. 4. (a) Output power of metasurface at different displacement ranges of 235 μm and 2030 μm. The slope indicating the measurement accuracy is improved by 10 times. k_0 denotes the point of maximum slope on the curve, which defines the region of peak sensitivity. (b) Measurement results at the position corresponding to maximum slope, indicating the best displacement measurement resolution. (c, d) Results of displacement measurements corresponding to different incident angles.

achieved nanoscale precision for spots of arbitrary size. In the future, we will focus on applying this technology to practical applications and further enhancing its accuracy.

$$\text{Achievable limit} = \frac{P_{\min}}{K_{\max}} \quad (12)$$

where P_{\min} denotes the detection accuracy of the sensor.

5. Conclusion

In this study, we have demonstrated a novel quantum metrology approach utilizing metasurface-enabled mode conversion to achieve sub-diffraction-limit displacement measurements. By employing a metasurface designed to convert an incident Gaussian beam into higher-order TEM modes, we successfully implemented a high-precision displacement sensing technique with an experimental resolution reaching 1 nm. The theoretical analysis, supported by Fisher information calculations, confirmed that the measurement accuracy remains stable even below the diffraction limit.

Compared to traditional optical interferometry and grating-based displacement sensors, our method offers distinct advantages, including simplified optical architecture, high robustness, and cost-effective integration. The ability to achieve picometer-level sensitivity without relying on complex multi-beam interference or large-scale nanostructure fabrication makes this approach particularly attractive for applications in precision metrology,

semiconductor lithography, and high-resolution microscopy. Furthermore, our results suggest that with optimized experimental configurations, including enhanced detection sensitivity and reduced environmental noise, even higher measurement resolutions can be attained.

Future work will focus on expanding this technique to large-range, multi-degree-of-freedom displacement measurements and integrating it into practical applications such as real-time wafer stage monitoring in EUV lithography. Additionally, incorporating advanced quantum measurement strategies, such as squeezed light injection and quantum-enhanced signal processing, could further push the limits of measurement accuracy. The proposed metasurface-based quantum metrology scheme not only provides a valuable tool for ultra-precision displacement sensing but also paves the way for broader advancements in quantum-enhanced optical measurement technologies.

CRedit authorship contribution statement

Wenyi Ye: Writing – original draft. **Yang Li:** Project administration, Conceptualization. **Lianwei Chen:** Project administration, Conceptualization. **Mingbo Pu:** Investigation. **Zheting Meng:** Writing – review & editing. **Yuanjian Huang:** Software. **Hengshuo Guo:** Writing – review & editing. **Xiaoyin Li:** Writing – review & editing. **Yinghui Guo:** Writing – review & editing. **Xiong Li:** Writing – review & editing, Investigation. **Yun Long:** Writing – review & editing.

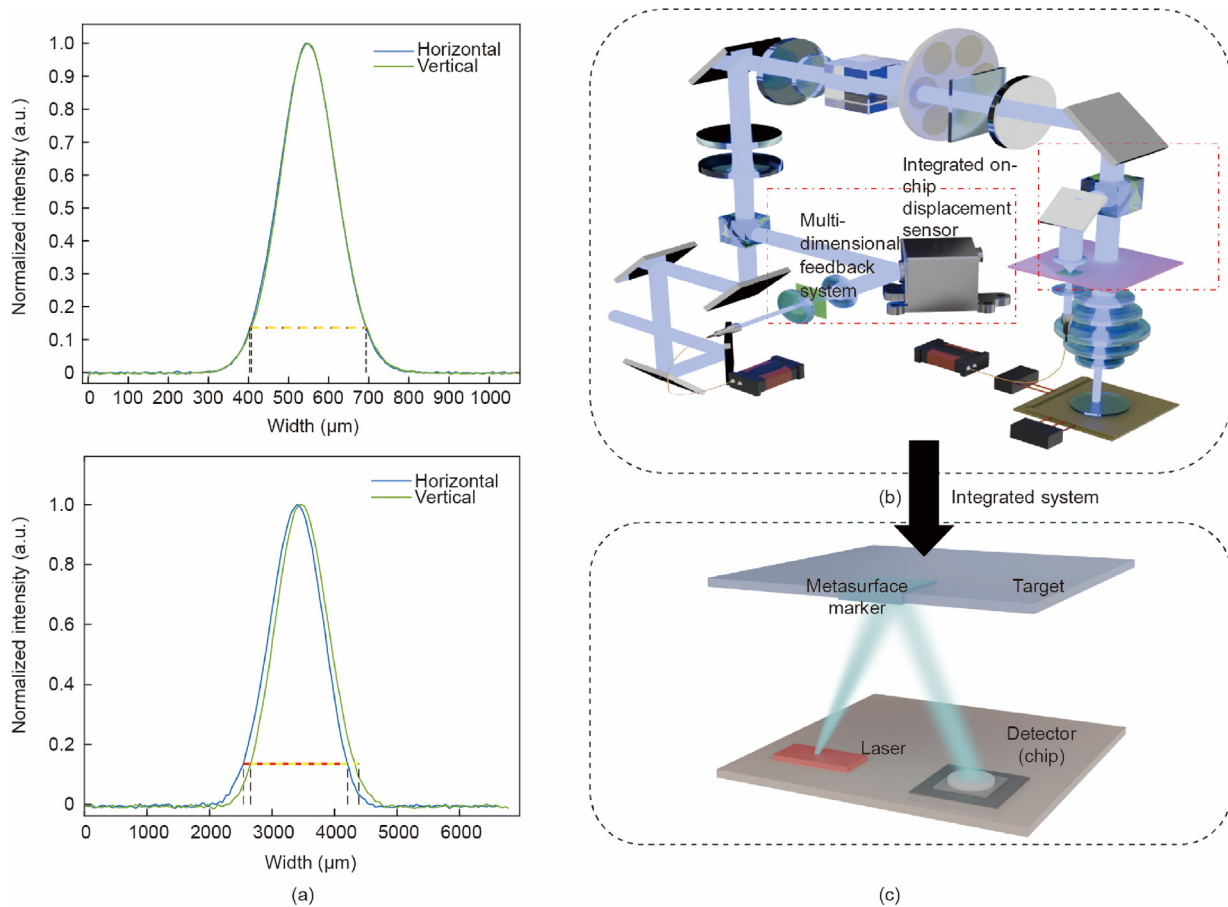


Fig. 5. (a) Different displacement measurements by the variation of this metasurface quantum sensor for practical applications. (b) Design of high accuracy motion sensor in optical nanofabrication systems. (c) Integrated on-chip displacement quantum sensors.

Emmanuel Stratakis: Writing – review & editing. **Xiangang Luo:** Writing – review & editing, Investigation.

Declaration of competing interest

The authors declare that they have no known competing financial interests or personal relationships that could have appeared to influence the work reported in this paper.

Acknowledgments

This work was supported by the West Light Project, CAS (xbzg-zdsys-202206), the National Key Research and Development Program of China (2021YFA1401003), the National Natural Science Foundation of China (NSFC) (62222513, U24A6010, and U24A20317), and the Sichuan Engineering Research Center of Digital Materials.

Appendix A. Supplementary data

Supplementary data to this article can be found online at <https://doi.org/10.1016/j.eng.2025.04.010>.

References

- [1] Xu J, Mao Y, Li Z, Zuo Y, Zhang J, Yang B, et al. Single-cavity loss-enabled nanometrology. *Nat Nanotechnol* 2024;19:1472–7.
- [2] Abbott BP, Abbott R, Abbott TD, Abernathy MR, Acernese F, Ackley K, et al. Observation of gravitational waves from a binary black hole merger. *Phys Rev Lett* 2016;116(6):061102.
- [3] Biercuk MJ, Uys H, Britton JW, Van Devender AP, Bollinger JJ. Ultrasensitive detection of force and displacement using trapped ions. *Nat Nanotechnol* 2010;5(9):646–50.
- [4] Chien MH, Steurer J, Sadeghi P, Cazier N, Schmid S. Nanoelectromechanical position-sensitive detector with picometer resolution. *ACS Photonics* 2020;7(8):2197–203.
- [5] Knobel RG, Cleland AN. Nanometre-scale displacement sensing using a single electron transistor. *Nature* 2003;424(6946):291–3.
- [6] Krieg M, Fläschner G, Alsteens D, Gaub BM, Roos WH, Wuite GJL, et al. Atomic force microscopy-based mechanobiology. *Nature Rev Phys* 2019;1(1):41–57.
- [7] Song QL, Li Y, Zhou ZY, Xiao YW, Yang JS, Huang LH, et al. High-precision ground measurement technology research for measuring pointing deviation in space-based gravitational wave detection telescopes. *Opto-Electron Eng* 2024;51(2):230234.
- [8] de Groot PJ. A review of selected topics in interferometric optical metrology. *Rep Prog Phys* 2019;82(5):056101.
- [9] Du J, Lin JB, Quan HY, Hu S. Displacement measurement analysis in distortion detection of lithography projection objective. *Opto-Electron Eng* 2023;50(2):220226.
- [10] Hertzberg JB, Rocheleau T, Ndikum T, Savva M, Clerk AA, Schwab KC. Back-action-evading measurements of nanomechanical motion. *Nat Phys* 2010;6(3):213–7.
- [11] LaRose R, Tikku A, O’Neel-Judy É, Cincio L, Coles PJ. Variational quantum state diagonalization. *npj Quantum Inf* 2019;5(1):57.
- [12] Zang H, Xi Z, Zhang Z, Lu Y, Wang P. Ultrasensitive and long-range transverse displacement metrology with polarization-encoded metasurface. *Sci Adv* 2022;8(41):eadd1973.
- [13] Zang H, Zhang Z, Huang Z, Lu Y, Wang P. High-precision two-dimensional displacement metrology based on matrix metasurface. *Sci Adv* 2024;10(2):eadk2265.
- [14] Barboza R, Babazadeh A, Marrucci L, Cardano F, de Lisió C, D’Ambrosio V. Ultrasensitive measurement of transverse displacements with linear photonic gears. *Nat Commun* 2022;13(1):1080.
- [15] Yap MJ, Cripe J, Mansell GL, McRae TG, Ward RL, Slagmolen BJJ, et al. Broadband reduction of quantum radiation pressure noise via squeezed light injection. *Nat Photonics* 2020;14(1):19–23.
- [16] Lu Q, Xiao Q, Liu C, Wang Y, Zhu Q, Xu M, et al. Inverse design and realization of an optical cavity-based displacement transducer with arbitrary responses. *Opto-Electron Adv* 2023;6(3):220018.

- [17] Hu P, Chang D, Tan J, Yang R, Yang H, Fu H. Displacement measuring grating interferometer: a review. *Front Inf Technol Electron Eng* 2019;20(5):631–54.
- [18] Rayleigh L. On the passage of waves through apertures in plane screens, and allied problems. *Lond Edinb Dublin Philos Mag J Sci* 1897;43(263):259–72.
- [19] Tsang M. Resolving starlight: a quantum perspective. *Contemp Phys* 2019;60(4):279–98.
- [20] Tsang M, Nair R, Lu XM. Quantum theory of superresolution for two incoherent optical point sources. *Phys Rev X* 2016;6(3):031033.
- [21] Tan XJ, Qi L, Chen L, Danner AJ, Kanchanawong P, Tsang M. Quantum-inspired superresolution for incoherent imaging. *Optica* 2023;10(9):1189–94.
- [22] Zhang JD, Fu Y, Hou L, Wang S. Superresolution imaging of two incoherent optical sources with unequal brightnesses. *Opt Express* 2024;32(15):26147–56.
- [23] Moreau PA, Toninelli E, Gregory T, Padgett MJ. Imaging with quantum states of light. *Nat Rev Phys* 2019;1(6):367–80.
- [24] Tenne R, Rossman U, Rephael B, Israel Y, Krupinski-Ptaszek A, Lapkiewicz R, et al. Super-resolution enhancement by quantum image scanning microscopy. *Nat Photonics* 2019;13(2):116–22.
- [25] Albarelli F, Barbieri M, Genoni MG, Gianani I. A perspective on multiparameter quantum metrology: from theoretical tools to applications in quantum imaging. *Phys Lett A* 2020;384(12):126311.
- [26] Paúr M, Stoklasa B, Hradil Z, Sánchez-Soto LL, Rehacek J. Achieving the ultimate optical resolution. *Optica* 2016;3(10):1144–7.
- [27] Nair R, Tsang M. Far-field superresolution of thermal electromagnetic sources at the quantum limit. *Phys Rev Lett* 2016;117(19):190801.
- [28] Lupo C, Pirandola S. Ultimate precision bound of quantum and subwavelength imaging. *Phys Rev Lett* 2016;117(19):190802.
- [29] Zanforlin U, Lupo C, Connolly PWR, Kok P, Buller GS, Huang Z. Optical quantum super-resolution imaging and hypothesis testing. *Nat Commun* 2022;13(1):5373.
- [30] Frank J, Duplinskiy A, Bearne K, Lvovsky AI. Passive superresolution imaging of incoherent objects. *Optica* 2023;10(9):1147–52.
- [31] Tsang M. Subdiffraction incoherent optical imaging via spatial-mode demultiplexing. *New J Phys* 2017;19(2):023054.
- [32] Tsang M. Quantum limit to subdiffraction incoherent optical imaging. *Phys Rev A* 2019;99(1):012305.
- [33] Unternährer M, Bessire B, Gasparini L, Perenzoni M, Stefanov A. Super-resolution quantum imaging at the heisenberg limit. *Optica* 2018;5(9):1150–4.
- [34] Yu Z, Prasad S. Quantum limited superresolution of an incoherent source pair in three dimensions. *Phys Rev Lett* 2018;121(18):180504.
- [35] Astratov VN, Sahel YB, Eldar YC, Huang L, Ozcan A, Zheludev N, et al. Roadmap on label-free super-resolution imaging. *Laser Photonics Rev* 2023;17(12):2200029.
- [36] Pushkina AA, Maltese G, Costa-Filho JI, Patel P, Lvovsky AI. Superresolution linear optical imaging in the far field. *Phys Rev Lett* 2021;127(25):253602.
- [37] Schlichtholz K, Rudnicki Ł. Superresolution in separation estimation between two dynamic incoherent sources using spatial demultiplexing. 2024. arXiv:2407.10507.
- [38] Sajja A, Qian XF. Superresolution of two unbalanced point sources assisted by the entangled partner. *Phys Rev Res* 2022;4(3):033244.
- [39] Tham WK, Ferretti H, Steinberg AM. Beating rayleigh's curse by imaging using phase information. *Phys Rev Lett* 2017;118(7):070801.
- [40] Luo XG. Principles of electromagnetic waves in metasurfaces. *Sci China Phys Mech Astron* 2015;58(9):594201.
- [41] Xie X, Pu M, Jin J, Xu M, Guo Y, Li X, et al. Generalized Pancharatnam–Berry phase in rotationally symmetric meta-atoms. *Phys Rev Lett* 2021;126(18):183902.
- [42] Wang X, Wang H, Wang J, Liu X, Hao H, Tan YS, et al. Single-shot isotropic differential interference contrast microscopy. *Nat Commun* 2023;14(1):2063.
- [43] Wang X, Hao H, He X, Xie P, Liu J, Tan J, et al. Advances in information processing and biological imaging using flat optics. *Nat Rev Electr Eng* 2024;1:391–411.
- [44] Hao H, Wang H, Wang X, Ding X, Zhang S, Pan CF, et al. Single-shot 3D imaging meta-microscope. *Nano Lett* 2024;24(42):13364–73.
- [45] Luo X. Subwavelength artificial structures: opening a new era for engineering optics. *Adv Mater* 2019;31(4):1804680.
- [46] Li X, Chen L, Li Y, Zhang X, Pu M, Zhao Z, et al. Multicolor 3D meta-holography by broadband plasmonic modulation. *Sci Adv* 2016;11(2):e1601102.
- [47] Zhang F, Guo Y, Pu M, Chen L, Xu M, Liao M, et al. Meta-optics empowered vector visual cryptography for high security and rapid decryption. *Nat Commun* 2023;14(1):1946.
- [48] Zheng C, Wang G, Li J, Li J, Wang S, Zhao H, et al. All-dielectric metasurface for manipulating the superpositions of orbital angular momentum via spin-decoupling. *Adv Opt Mater* 2021;9(10):2002007.
- [49] Ahmed H, Intaravanne Y, Ming Y, Ansari MA, Buller GS, Zentgraf T, et al. Multichannel superposition of grafted perfect vortex beams. *Adv Mater* 2022;34(30):2203044.
- [50] Yoon G, Lee D, Nam KT, Rho J. Pragmatic metasurface hologram at visible wavelength: the balance between diffraction efficiency and fabrication compatibility. *ACS Photonics* 2018;5(5):1643–7.
- [51] Cai H, Czaplowski D, Ogando K, Martinson A, Gosztola D, Stan L, et al. Ultrathin transmissive metasurfaces for multi-wavelength optics in the visible. *Appl Phys Lett* 2019;114(7):071106.
- [52] Arbabi E, Arbabi A, Kamali SM, Horie Y, Faraon A. High efficiency double-wavelength dielectric metasurface lenses with dichroic birefringent meta-atoms. *Opt Express* 2016;24(16):18468–77.
- [53] Yu YF, Zhu AY, Paniagua-Domínguez R, Fu YH, Luk'yanchuk B, Kuznetsov AI. High-transmission dielectric metasurface with 2π phase control at visible wavelengths. *Laser Photonics Rev* 2015;9(4):412–8.
- [54] Arbabi E, Arbabi A, Kamali SM, Horie Y, Faraon A. Multiwavelength metasurfaces through spatial multiplexing. *Sci Rep* 2016;6(1):32803.
- [55] Chen WT, Khorasaninejad M, Zhu AY, Oh J, Devlin RC, Zaidi A, et al. Generation of wavelength-independent subwavelength Bessel beams using metasurfaces. *Light Sci Appl* 2017;6(5):e16259.
- [56] Wang QS, Fang Y, Meng Y, Hao H, Li X, Pu M, et al. Vortex-field enhancement through high-threshold geometric metasurface. *Opto-Electron Adv* 2024;7(12):240112.
- [57] Liu Q, Pierce DA. A note on Gauss–Hermite quadrature. *Biometrika* 1994;81(3):624–9.
- [58] Kang D, Heo H, Yang Y, Seong J, Kim H, Kim J, et al. Liquid crystal-integrated metasurfaces for an active photonic platform. *Opto-Electron Adv* 2024;7(6):230216.
- [59] Yang Y, Forbes A, Cao L. A review of liquid crystal spatial light modulators: devices and applications. *Opto-Electron Sci* 2023;2(8):230026.
- [60] Helstrom CW. Quantum detection and estimation theory. *J Stat Phys* 1969;1:231–52.
- [61] Braunstein SL, Caves CM. Statistical distance and the geometry of quantum states. *Phys Rev Lett* 1994;72(22):3439–43.